applied optics

Polarization-independent plasmonic subtractive color filtering in ultrathin Ag nanodisks with high transmission

X. L. Hu,[1,†] L. B. Sun,[1,†] Beibei Zeng,[2,3] L. S. Wang,[4] Z. G. Yu,[5] S. A. Bai,[1] S. M. Yang,[4] L. X. Zhao,[5] Q. Li,[1] M. Qiu,[1] R. Z. Tai,[4] H. J. Fecht,[6] J. Z. Jiang,[7] and D. X. Zhang[1,*]

[1]State Key Laboratory of Modern Optical Instrumentation, Zhejiang University, Hangzhou 310027, China
[2]Department of Electrical and Computer Engineering, Lehigh University, Bethlehem, Pennsylvania 18015, USA
[3]Currently at Center for Integrated Nanotechnologies, Los Alamos National Laboratory, Los Alamos, New Mexico 87545, USA
[4]Shanghai Institute of Applied Physics, Chinese Academy of Sciences, Shanghai 201204, China
[5]Institute of Semiconductors, Chinese Academy of Sciences, Beijing 100083, China
[6]Department of Materials, Faculty of Engineering, University of Ulm, Albert-Einstein Allee 47, D-89081 Ulm, Germany
[7]International Center for New-Structured Materials, State Key Laboratory of Silicon Materials and Department of Materials Science and Engineering, Zhejiang University, Hangzhou 310027, China
*Corresponding author: zhangdx@zju.edu.cn

Received 11 September 2015; revised 3 November 2015; accepted 24 November 2015; posted 25 November 2015 (Doc. ID 249926); published 23 December 2015

We demonstrate a TE/TM polarization-independent plasmonic subtractive color filtering scheme employing ultrathin two-dimensional Ag nanodisks. These TE/TM polarization-independent subtractive color filters exhibit small feature sizes (below 200 nm) and high transmission up to 70% in the visible spectral region, superior to previously reported plasmonic color filters. Simulated optical transmission spectra and colors are in good agreement with experimental results. The color-filtering behaviors strongly depend on thickness and period of nanodisks. Underlying mechanisms are also discussed in detail.

OCIS codes: (120.7000) Transmission; (240.0310) Thin films; (260.5430) Polarization; (310.6628) Subwavelength structures, nanostructures.

http://dx.doi.org/10.1364/AO.55.000148

Extraordinary low transmission (ELT) through ultrathin nanostructured metallic films, where the thickness of metal film is comparable to or below its skin depth, has sparked intense interest and applications recently [1–4]. When an ultrathin metal film is patterned with periodic arrays of nanoapertures, one may intuitively expect that it could transmit more light because some of the light-blocking metals are removed. Surprisingly, previous works indicate that the light transmission within certain spectral bands can be totally suppressed. This is exactly in opposition to the well-known extraordinary optical transmission (EOT) of light through optically thick (beyond the skin depth) metal films patterned with periodic arrays of subwavelength apertures [5,6]. The EOT phenomenon is induced by the resonant coupling of photons to surface plasmons at a metal–dielectric boundary, which is strongly related to the type of metal and dielectric and subwavelength structures [7–9]. This provides an efficient method for light manipulation by changing the materials or geometric parameters of subwavelength structures. Plasmonic additive color filters (ACFs) were then proposed using the EOT phenomenon to filter red, green, and blue colors. Due to the advantages of good reliability, environmental friendliness, and durability, plasmonic ACFs are superior to traditional color filters using chemical pigments or dyes, making them promising components for image sensors, digital cameras, projectors, and other optical measurement instrumentation [10–15]. However, there remain several restrictions for industrial applications such as low transmission efficiency (~30%) and complex, high-cost fabrication processes. Therefore, further improvement of this technique is strongly desired [7, 8, 16,17]. On the other hand, for the ELT phenomenon, one of the most promising applications is plasmonic subtractive color filters (SCFs) in which cyan, magenta, and yellow subtractive colors can be achieved. Recently, Zeng *et al.* [18] reported a simple one-layer Ag film (30 nm in thickness) with subwavelength patterns acting as plasmonic SCFs, achieving high transmission efficiency (about 60%). This is a very attractive approach for industrial applications.

In our previous work, the effects of film thickness and period on color filtering in ultrathin Ag nanograting and nanohole arrays were systematically studied [19]. It was found that

the transmission minimum wavelength exhibits a redshift with increasing period and decreasing film thickness. Color-filtering behaviors strongly depend on geometric parameters of the patterned nanostructures, e.g., hole shape [20], inner coaxial particles in the hole [21,22], and layer separation distance [23]. Most recently, ELT phenomena through two-dimensional Au nanodisks [24] and Al nanopatches [25] have been reported in which the ELT effect in Au nanodisks is only observed in the near-infrared region and the feature sizes for both Au nanodisks and Al nanopatches are larger than 200 nm (or half of the wavelength from 400 to 700 nm). Since the pixel size is a critical concern for applications such as high-density information storage and high-resolution image sensors, it is still strongly desirable to design plasmonic color filters with *smaller feature sizes* (below 200 nm) in *the visible spectral region*. In this work, we propose polarization-independent plasmonic SCFs utilizing ultrathin Ag nanodisks with various structural parameters. A series of ultrathin Ag nanodisk-based plasmonic SCFs are first fabricated and characterized. High transmission efficiency of up to 70% in the visible region and the period down to 140–200 nm are achieved in these Ag nanodisk plasmonic SCFs. A systematic study is performed to clarify the dependence of color-filtering behaviors on the thickness and period of Ag nanodisks. The same simulated transmission spectra of the proposed plasmonic SCFs under both transverse-electric (TE) and transverse-magnetic (TM) polarized illuminations indicate their polarization-independent functionality [26].

Figure 1(a) illustrates ultrathin Ag nanodisks on a glass substrate. Here, P is the period, d represents the thickness, L is the diameter, and the ratio $r = L/P$ is 0.5. For the preparation of two-dimensional Ag nanodisk arrays [27], Ag films on glass substrate (roughness of about 1 nm) were magnetron-sputtered using a direct-current magnetron sputtering system (JZCK-400) in a vacuum of 5×10^{-4} Pa chamber under purified argon atmosphere of 0.5 Pa. The bulk Ag target material with a purity of 99.999 at. % was sputtered using the voltage of 420 V and current of 0.15 A. The thickness of deposited films was characterized by spectroscopic ellipsometer (Semilab Sopra GES_5E) and synchrotron radiation x-ray reflectivity (SR-XRR) at beamline BL14B1 of the Shanghai Synchrotron Radiation Facility at a wavelength of 0.124 nm. The film thickness is determined to be 40 nm. Nanodisk arrays were fabricated using an electron beam lithography system. The size of the studied Ag nanodisk arrays is 120 μm × 120 μm. Their microstructures were monitored by field emission scanning electron microscopy (Hitachi S-4800). Figure 1(b) is the SEM image for 40 nm thick Ag nanodisks with a period of 290 nm. Optical microscopy images of nanodisk arrays under white light were measured using a standard microscope (Nikon 80i).

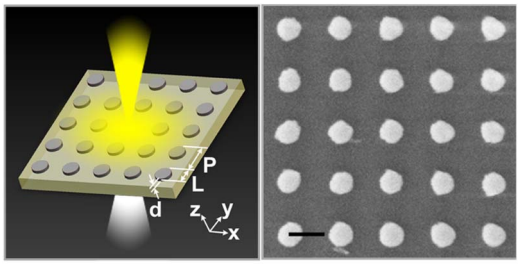

Fig. 1. (a) Illustration of the studied nanodisk structure for metallic Ag film on glass. P is the period of the nanodisks, d represents the thickness of the ultrathin Ag films, L is the diameter of the nanodisks, and the ratio $r = L/P$ is 0.5. (b) SEM image for 40 nm thick Ag nanodisks with a period of 290 nm. The scale bar is 200 nm.

Using the FDTD method, we simulated transmission spectra through Ag nanodisk arrays for different film thicknesses and periods. The complex dielectric constants n and k used in the simulations were from Palik [28], in which a series of n and k data experimentally determined at different wavelengths for Ag films were fitted with a tolerance of 0.01 and max coefficient of 3. In order to fully absorb scattered light, perfect matched layer (PML) boundary conditions were used in simulations. Symmetric or antisymmetric boundary conditions were also applied to obtain the periodic structure and reduce the computing time. The selection of symmetric or antisymmetric boundary condition was related to the polarization of the source, which was a white light plane source with a band of 400–750 nm. If the source was TM-polarized, $x_{\min}$ and $x_{\max}$ boundaries were set to antisymmetric boundary conditions, $y_{\min}$ and $y_{\max}$ boundaries were set to symmetric boundary conditions, while $z_{\min}$ and $z_{\max}$ boundaries were set to PML boundary conditions. Otherwise, the source was TE-polarized and $x_{\min}$ and $x_{\max}$ boundaries were set to symmetric boundary conditions, $y_{\min}$ and $y_{\max}$ boundaries were set to antisymmetric boundary conditions, and $z_{\min}$ and $z_{\max}$ boundaries were set to PML boundary conditions. To ensure convergence, the simulations were performed for different mesh sizes of 5, 4, 3, 2, 1, and 0.5 nm, and the results (transmission spectra) converged as the mesh size varied from 1 to 0.5 nm. A 1 nm mesh grid was eventually chosen, as the results were reliable and resource occupation is acceptable at the same time.

A series of Ag nanodisk-based SCFs with periods ranging from 140 to 320 nm were fabricated. Figure 2(a) shows optical micrographs of all color filters under white light illumination. Using the FDTD method, transmission spectra for Ag nanodisks with periods P from 140 to 360 nm in steps of 10 nm, d from 10 to 50 nm in steps of 5 nm, and r of 0.5 were also obtained. Figure 2(b) shows the CIE1931 chromaticity diagram overlaid with points corresponding to colors calculated by the simulated transmission spectra for 40 nm thick Ag nanodisks (P = 140, 170, 180, 210, 240, 260, 290, 310, and 320 nm) under white light illumination. More specifically, the coordinates of the color for each simulated transmission spectra on the CIE1931 chromaticity diagram was calculated by substituting Eqs. (1)–(4) into Eqs. (5) and (6):

$$X = k\sum_{\lambda}\beta(\lambda)P(\lambda)\bar{x}(\lambda), \tag{1}$$

$$Y = k\sum_{\lambda}\beta(\lambda)P(\lambda)\bar{y}(\lambda), \tag{2}$$

$$Z = k\sum_{\lambda}\beta(\lambda)P(\lambda)\bar{z}(\lambda), \tag{3}$$

$$k = 100/\sum_{\lambda}P(\lambda)\bar{y}(\lambda), \tag{4}$$

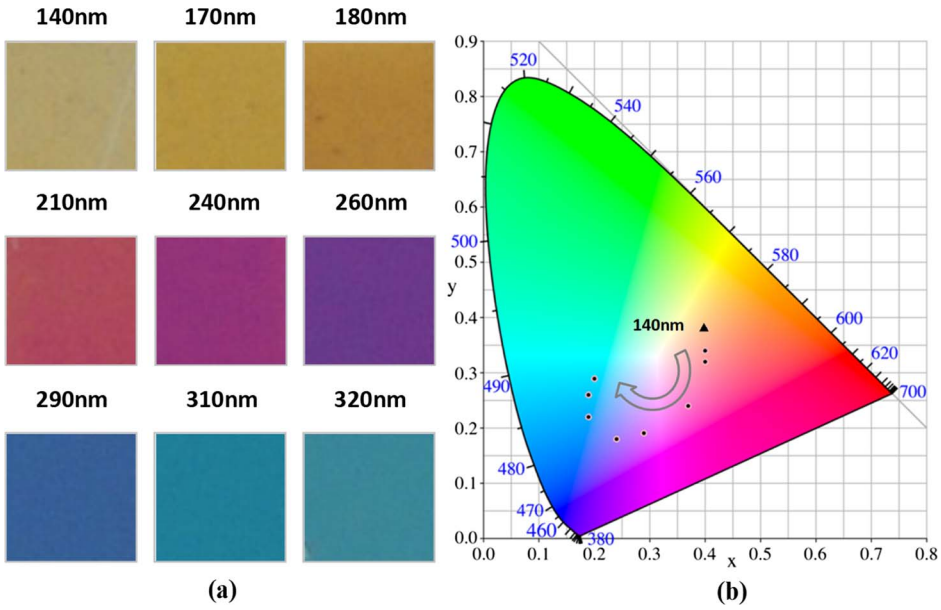

Fig. 2. (a) Optical micrographs. (b) CIE1931 chromaticity diagrams overlaid with points corresponding to the simulated transmission spectra colors for 40 nm thick Ag nanodisks with periods $P = 140$, 170, 180, 210, 240, 260, 290, 310, and 320 nm and $r = 0.5$ under white light illumination.

$$x = X/(X + Y + Z), \tag{5}$$

$$y = Y/(X + Y + Z), \tag{6}$$

where $\beta(\lambda)$ is the transmission spectra, $P(\lambda)$ is the spectra of source, and $\bar{x}(\lambda)$, $\bar{y}(\lambda)$, and $\bar{z}(\lambda)$ represent tristimulus values. The value of λ is from 400 to 750 nm in a step of 1 nm here, and (x, y) is the chromaticity coordinate for a given transmission spectra.

In Fig. 2(b), the point marked with a triangle stands for the chromaticity coordinates of Ag nanodisks with 140 nm period, and the arc arrow in Fig. 2(b) shows the trend of chromaticity coordinates by changing periods from 140 to 320 nm. The simulated results are in good agreement with the observed colors in Fig. 2(a). Figure 3(a) shows the simulated transmission spectra of the 40 nm thick Ag nanodisks with P from 140 to 360 nm in steps of 10 nm. The transmission minimum exhibits a redshift with increasing periods. Figure 3(b) shows the simulated transmission spectra of nanodisks with $P = 290$, 310, and 320 nm and $r = 0.5$ for 40 nm Ag film and Fig. 3(c) shows the measured transmission spectra of nanodisks with $P = 290$, 310, and 320 nm and $r = 0.5$ for 40 nm Ag film obtained under a normally incident and unpolarized white light illumination with an 80 μm sized light spot. The simulated transmission spectrum shows reasonable agreement with the experiment, although the spectrum was measured in a wavelength span starting from 500 nm due to the limitation of our optical setup. The influence of light with other polarization angles could be the reason for the difference between the measured transmission spectrum and the simulated one. From the measured transmission spectrum, it is found that ultrathin Ag nanodisk arrays can exhibit high transmission efficiency of up to 70%.

To dig further into the physical origin for the ELT phenomenon observed here, a 2D transmission spectrum map for 40 nm thick Ag nanodisks as a function of period and incident wavelength is plotted in Fig. 4(a), together with the contributions of short-range surface plasmon polaritons (SRSPPs, solid white line) and localized surface plasmon

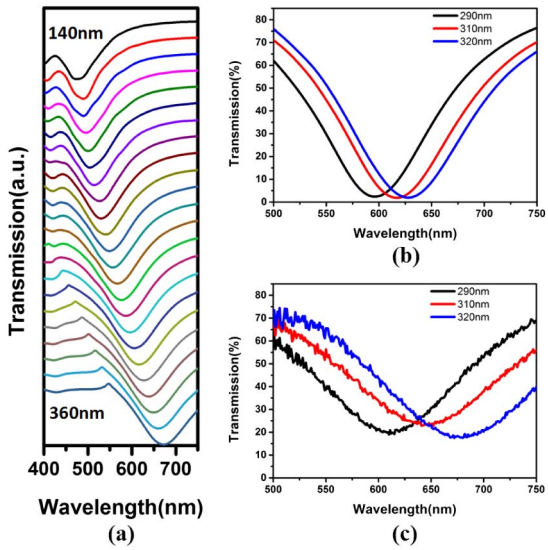

Fig. 3. (a) Transmission spectra of nanodisks with $r = 0.5$ and P ranging from 140 to 360 nm in steps of 10 nm for 40 nm Ag film. The transmission minimum clearly exhibits a redshift with increasing period. (b) Simulated transmission spectra of nanodisks with $r = 0.5$ and $P = 290$, 310, and 320 nm for 40 nm Ag film. (c) Measured transmission spectra of nanodisks with $r = 0.5$ and $P = 290$, 310, and 320 nm for 40 nm Ag film obtained by a system with an 80 μm sized light spot under normal incidence unpolarized white light illumination.

polaritons (LSPPs, dashed white line). The resonance wavelength of SRSPPs was calculated by the analytical dispersion relations for ultrathin Ag films patterned with periodic nanostructures [29]:

$$\tanh(k_2 d)(\varepsilon_{d1}\varepsilon_{d2}k_2^2 + \varepsilon_m^2 k_1 k_3) + \varepsilon_m k_2(\varepsilon_{d1}k_3 + \varepsilon_{d2}k_1) = 0, \tag{7}$$

where

$$k_1^2 = k_{\text{spp}}^2 - \varepsilon_{d1}k_0^2, \tag{8}$$

$$k_2^2 = k_{\text{spp}}^2 - \varepsilon_m k_0^2, \tag{9}$$

$$k_3^2 = k_{\text{spp}}^2 - \varepsilon_{d2}k_0^2. \tag{10}$$

Here, d is the thickness of the metal film. ε_{d1} and ε_{d2} are dielectric constants of air and glass, respectively, and ε_m represents the dielectric constant of ultrathin Ag film. In addition,

$$k_{\text{spp}} = k_0 \sin\theta + nG_x + mG_y, \tag{11}$$

where

$$G_x = G_y = 2\pi/P. \tag{12}$$

Here, P is the period of the nanodisk array, m is an integer, and θ is the incident angle. For normal incidence ($\theta = 0°$), the dispersion relation of the SRSPP mode was obtained by substituting Eqs. (8)–(12) into Eq. (7).

The resonance wavelength of the LSPPs was obtained by simulation for a single Ag nanodisk with the same size as that of the nanodisk array. It is found that the low-transmission band and the contributions of SRSPPs and LSPPs have a similar dependence on the period, i.e., they shift to longer wavelengths with increasing period. Obviously, LSPPs fit to the transmission dip of the nanodisk array well, indicating that LSPPs could be the major contribution to the observed ELT phenomenon for the Ag nanodisk array. This is quite different from the Ag nanograting array, for which both SRSPPs and LSPPs contribute to the ELT phenomenon as mentioned in Ref. [18]. Furthermore, 2D maps of reflection and absorption are also given in Figs. 4(b) and 4(c), together with the SRSPP and LSPP resonance wavelengths plotted in solid and dashed white lines, respectively. Figures 4(a)–4(c) show that the transmission minimum is primarily attributed to enhanced absorption and reflection in the Ag nanodisk array. For periods smaller than about 250 nm, the transmission minimum is mainly linked with the enhanced absorption whereas, for periods greater than 250 nm, the enhanced reflection is the main factor. To further characterize the electromagnetic modes at the resonance wavelength, we calculated the electric field distributions for Ag nanodisks with a 290 nm period at a resonance wavelength of 596 nm in Fig. 4(d), and indeed found excitation of LSPPs.

In conclusion, TE/TM polarization-independent plasmonic subtractive color filters with small feature size (below 200 nm)

and high transmission (up to 70%) in the visible spectral region were successfully demonstrated by employing extraordinarily low transmission phenomena in two-dimensional ultrathin Ag nanodisks. The dependence of color-filtering behaviors on thickness and period of nanodisks have been systematically investigated. It is found that color-filtering behaviors strongly correlate with the thickness and period of nanodisks. The localized surface plasmon polaritons, rather than short-range surface plasmon polaritons, could be the key factor in the extraordinarily low transmission phenomenon in this scheme. The obtained results are significant for designing plasmonic subtractive color filters by selecting appropriate geometric parameters for Ag nanodisks. The proposed TE/TM polarization-independent plasmonic color filters with small feature size and high transmission over visible spectral band are promising for digital imaging, information storage, and sensing.

Funding. China Scholarship Council (CSC) (201400260166); National Key Basic Research Program of China (2012CB825700); National Natural Science Foundation of China (NSFC) (51371157, U1432105, U1432110); Open Research Project of Large Scientific Facility of the Chinese Academy of Sciences (CAS): Study on Self-assembly Technology and Nanometer Array with Ultra-high Density.

Acknowledgment. The authors acknowledge the support of Soft-X Ray Interference Lithography Beamline (BL08U1B) in SSRF for sample preparation, and the support from Open Research Project of Large Scientific Facility from Chinese Academy of Sciences: Study on Self-assembly Technology and Nanometer Array with Ultra-high Density.

†These authors contributed equally to this work.

REFERENCES

1. I. S. Spevak, A. Y. Nikitin, E. V. Bezuglyi, A. Levchenko, and A. V. Kats, "Resonantly suppressed transmission and anomalously enhanced light absorption in periodically modulated ultrathin metal films," Phys. Rev. B **79**, 161406 (2009).
2. G. D'Aguanno, N. Mattiucci, A. Alu, and M. J. Bloemer, "Quenched optical transmission in ultrathin subwavelength plasmonic gratings," Phys. Rev. B **83**, 035426 (2011).
3. B. B. Zeng, Y. K. Gao, and F. J. Bartoli, "Rapid and highly sensitive detection using Fano resonances in ultrathin plasmonic nanogratings," Appl. Phys. Lett. **105**, 161106 (2014).
4. B. B. Zeng, Z. H. Kafafi, and F. J. Bartoli, "Transparent electrodes based on two-dimensional Ag nanogrids and double one-dimensional Ag nanogratings for organic photovoltaics," J. Photon. Energy **5**, 057005 (2015).
5. F. J. García de Abajo, "Colloquium: light scattering by particle and hole arrays," Rev. Mod. Phys. **79**, 1267–1290 (2007).
6. F. J. Garcia-Vidal, L. Martin-Moreno, T. W. Ebbesen, and L. Kuipers, "Light passing through subwavelength apertures," Rev. Mod. Phys. **82**, 729–787 (2010).
7. W. L. Barnes, A. Dereux, and T. W. Ebbesen, "Surface plasmon subwavelength optics," Nature **424**, 824–830 (2003).
8. Q. Chen and D. Cumming, "High transmission and low color cross-talk plasmonic color filters using triangular-lattice hole arrays in aluminum films," Opt. Express **18**, 14056–14062 (2010).
9. S. Yokogawa, S. P. Burgos, and H. A. Atwater, "Plasmonic color filters for CMOS image sensor applications," Nano Lett. **12**, 4349–4354 (2012).
10. S. Landis, P. Brianceau, V. Reboud, N. Chaix, Y. Désières, and M. Argoud, "Metallic colour filtering arrays manufactured by nanoimprint lithography," Microelectron. Eng. **111**, 193–198 (2013).
11. A. Boltasseva, S. I. Bozhevolnyi, T. Sondergaard, T. Nikolajsen, and K. Leosson, "Compact Z-add-drop wavelength filters for long-range surface plasmon polaritons," Opt. Express **13**, 4237–4243 (2005).
12. V. S. Volkov, S. I. Bozhevolnyi, E. Devaux, J. Y. Laluet, and T. W. Ebbesen, "Wavelength selective nanophotonic components utilizing channel plasmon polaritons," Nano Lett. **7**, 880–884 (2007).
13. E. Laux, C. Genet, T. Skauli, and T. W. Ebbesen, "Plasmonic photon sorters for spectral and polarimetric imaging," Nat. Photonics **2**, 161–164 (2008).
14. T. W. Ebbesen, H. J. Lezec, H. F. Ghaemi, T. Thio, and P. A. Wolff, "Extraordinary optical transmission through sub-wavelength hole arrays," Nature **391**, 667–669 (1998).
15. C. Genet and T. W. Ebbesen, "Light in tiny holes," Nature **445**, 39–46 (2007).
16. S. Collin, G. Vincent, R. Haïdar, N. Bardou, S. Rommeluère, and J. L. Pelouard, "Nearly perfect fano transmission resonances through nanoslits drilled in a metallic membrane," Phys. Rev. Lett. **104**, 027401 (2010).
17. H. F. Ghaemi, T. Thio, D. E. Grupp, T. W. Ebbesen, and H. J. Lezec, "Plasmonic photon sorters for spectral and polarimetric imaging," Phys. Rev. B **58**, 6779–6782 (1998).
18. B. B. Zeng, Y. K. Gao, and F. J. Bartoli, "Ultrathin nanostructured metals for highly transmissive plasmonic subtractive color filters," Sci. Rep. **3**, 2840 (2013).
19. X. L. Hu, L. B. Sun, B. Shi, M. Ye, Y. Xu, L. S. Wang, J. Zhao, X. L. Li, Y. Q. Wu, S. M. Yang, R. Z. Tai, H. J. Fecht, J. Z. Jiang, and D. X. Zhang, "Influence of film thickness and nanograting period on color-filter behaviors of plasmonic metal Ag films," J. Appl. Phys. **115**, 113104 (2014).
20. K. J. Klein Koerkamp, S. Enoch, F. B. Segerink, N. F. van Hulst, and L. Kuipers, "Strong influence of hole shape on extraordinary transmission through periodic arrays of subwavelength holes," Phys. Rev. Lett. **92**, 183901 (2004).
21. S. Wu, Q. J. Wang, X. G. Yin, J. Q. Li, D. Zhu, S. Q. Liu, and Y. Y. Zhu, "Enhanced optical transmission: role of the localized surface plasmon," Appl. Phys. Lett. **93**, 101113 (2008).
22. M. D. He, J. Q. Liu, and X. S. Chen, "Light transmission through metallic two-dimensional arrays of compound," J. Appl. Phys. **106**, 113529 (2009).
23. J. Wang, Y. Zeng, X. S. Chen, W. Lu, and J. V. Moloney, "Various mechanisms for efficient optical transmission through bilayered subwavelength patterned metal films," J. Opt. Soc. Am. B **26**, B7–B10 (2009).
24. S. S. Xiao and N. A. Mortensen, "Surface-plasmon-polariton-induced suppressed transmission through ultrathin metal disk arrays," Opt. Lett. **36**, 37–39 (2011).
25. V. R. Shrestha, S. S. Lee, E. S. Kim, and D. Y. Choi, "Aluminum plasmonics based highly transmissive polarization-independent subtractive color filters exploiting a nanopatch array," Nano Lett. **14**, 6672–6678 (2014).
26. B. Gompf, J. Braun, T. Weiss, H. Giessen, M. Dressel, and U. Hübner, "Periodic nanostructures: spatial dispersion mimics chirality," Phys. Rev. Lett. **106**, 185501 (2011).
27. J. W. Menezes, J. Ferreira, M. Santos, L. Cescato, and A. G. Brolo, "Large-area fabrication of periodic arrays of nanoholes in metal films and their application in biosensing and plasmonic-enhanced photovoltaics," Adv. Funct. Mater. **20**, 3918–3924 (2010).
28. E. D. Palik, *Handbook of Optical Constants of Solids* (Academic, 1985).
29. J. Braun, B. Gompf, G. Kobiela, and M. Dressel, "How holes can obscure the view: suppressed transmission through an ultrathin metal film by a subwavelength hole array," Phys. Rev. Lett. **103**, 203901 (2009).